Interactions of vinca alkaloid subunits with chiral amido[4]resorcinarenes: a dynamic, kinetic, and spectroscopic study†

Bruno Botta,*[a] Caterina Fraschetti,[a] Francesca R. Novara,[b] Andrea Tafi,[c] Fabiola Sacco,[a] Luisa Mannina,[d,e] Anatoli P. Sobolev,[d] Jochen Mattay,[f] Matthias C. Letzel[f] and Maurizio Speranza*[a]

Received 15th January 2009, Accepted 15th January 2009
First published as an Advance Article on the web 4th March 2009
DOI: 10.1039/b900735k

The stereoselectivity of the reaction between (*R*)-(−)-2-butylamine and the diastereomeric proton-bound complexes of (+)-catharanthine (**C**) or (−)-vindoline (**V**) with some chiral amido[4]resorcinarenes has been investigated in the gas phase by ESI-FT-ICR-MS. The reaction stereoselectivity ($0.56 < k_{homo}/k_{hetero} < 16.9$) is found to depend critically on the functional groups present in the chiral pendants of the hosts. Rationalisation of the kinetic results is based on careful computational and spectroscopic studies of the most stable conformations of (+)-catharanthine and its protonated form in the isolated state and in water, as well as in a representative host structure. The emerging picture points to the relevant diastereomeric proton-bound complexes as quasi-degenerate, thus suggesting that their stereoselectivity in the guest exchange reaction is mostly due to kinetic factors. The results of this study may represent a starting point for a deeper comprehension of the intrinsic factors that endow these molecules, and their dimeric forms, with their biochemical properties.

Introduction

Vinblastine and vincristine are the most widely recognised members of the family of vinca alkaloids which are among the most powerful drug types currently in use for the clinical treatment of cancer.[1–3] Structurally, these two drugs, as well as others of the same family, are "dimeric" molecules, comprising two subunits, *i.e.* rearranged (+)-catharanthine (**C**) and (−)-vindoline (**V**) (Chart 1).

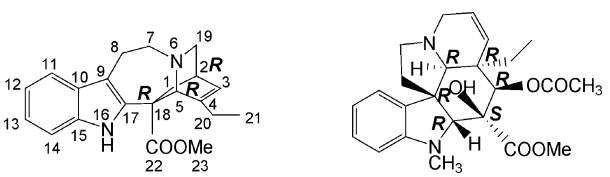

Chart 1 Chemical structures of vinca-alkaloid subunits (**A**).

In their "dimeric" form, these drugs induce tubulin to self-associate into linear polymers, thus inhibiting microtubule formation and mitosis. In comparison, the anticancer activity of the isolated subunits **V** and **C** is orders of magnitude lower than that of vinblastine and vincristine.[4] Nevertheless, it appears of interest to investigate the intrinsic properties of these components on a molecular level and to establish how much they are influenced by the physical environment. Furthermore, it would be of interest to study how **V** and **C** interact with some artificial receptors of defined structure and configuration in order to shed some light on the factors that endow these molecules, and their dimeric forms, with their corresponding biochemical properties.

We recently carried out extensive NMR[5,6] and mass spectrometric (MS) studies[5–13] on the interactions of some representative chiral biomolecules (**A**) with specifically designed chiral artificial receptors (**M**), such as the amido[4]resorcinarenes (Chart 2).

The molecular asymmetry of the selected hosts **M** is due to their dissymmetric pendants which may be spatially oriented so as to generate chiral cavities of different size and shape.[9] The enantioselectivity of the selected **M** hosts towards the **A** enantiomers was checked by introducing into a Fourier transform ion cyclotron resonance mass spectrometer (FT-ICR-MS), equipped with an electrospray ionisation source (ESI), the proton-bonded two-body complexes $[\mathbf{M}\cdot\mathbf{H}\cdot\mathbf{A}]^+$ and by measuring the rate of the displacement reaction 1 (eqn 1) where **B** is (*R*)-(−)-2-butylamine.

$$[\mathbf{M}\cdot\mathbf{H}\cdot\mathbf{A}]^+ + \mathbf{B} \rightarrow [\mathbf{M}\cdot\mathbf{H}\cdot\mathbf{B}]^+ + \mathbf{A} \quad (1)$$

The same kinetic approach is employed in the present paper in order to get an insight into the specific interactions between **A** = **C** or **V** and the two enantiomeric forms of several chiral macrocyclic hosts **M**, bearing either flexible, *i.e.* $\mathbf{1}_{R/S}$–$\mathbf{3}_{R/S}$, or rigid pendants, *i.e.* $\mathbf{4}_{R/S}$ and $\mathbf{5}_{R/S}$. The relevant kinetic results will be discussed in the light of molecular mechanics (MM) calculations and molecular

[a]*Dipartimento di Chimica e Tecnologie del Farmaco, Sapienza-Università di Roma, P.le A. Moro, 5-00185 Roma, Italy. E-mail: maurizio.speranza@uniroma1.it; Tel: +39-06-4991-3497; Fax: +39-06-49913497*
[b]*Institut für Chemie, Technische Universität Berlin, D-10623 Berlin, Germany*
[c]*Dipartimento Farmaco Chimico Tecnologico, Università di Siena, 53100 Siena, Italy*
[d]*Dipartimento di Scienze e Tecnologie Agro-Alimentari Ambientali e Microbiologiche (STAAM), Università del Molise, 86100 Campobasso, Italy*
[e]*Istituto di Metodologie Chimiche, CNR Area della Ricerca di Roma, Italy*
[f]*Department of Chemistry, Bielefeld University, 33501 Bielefeld, Germany*

† Electronic supplementary information (ESI) available: Kinetic plots of the gas-phase reaction between **B** and $[MHA]^+$ (A=catharanthine (**C**) or vindoline (**V**); $[\mathbf{4}_R\cdot H\cdot\mathbf{C}]^+$ and $[\mathbf{4}_S\cdot H\cdot\mathbf{C}]^+$ low-energy structures; NMR assignments; docking and molecular dynamics simulations: geometries and partial atomic charges. See DOI: 10.1039/b900735k

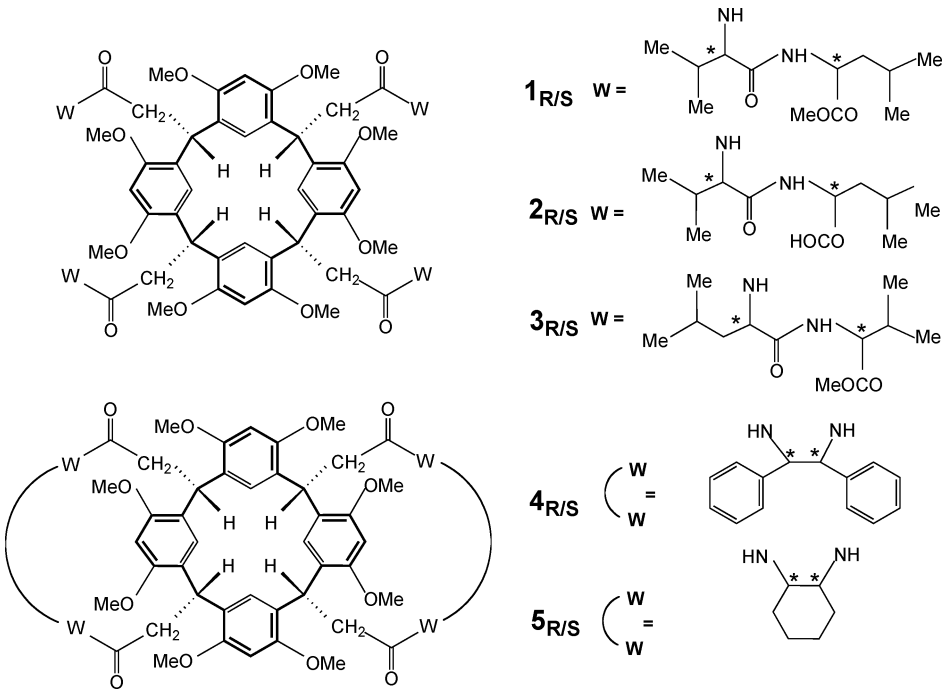

Chart 2 Chemical structures of the amido[4]resorcinarenes employed as chiral hosts (**M**).

dynamics (MD) simulations and compared with those obtained in previous related studies.

Results and discussion

FT-ICR-MS experiments

The proton-bound $[\mathbf{M}\cdot\mathbf{H}\cdot\mathbf{A}]^+$ complexes were generated in the FT-ICR-MS by electrospraying **M**/**A** methanolic solutions. The reaction of $[\mathbf{M}\cdot\mathbf{H}\cdot\mathbf{A}]^+$ with amine **B** leads to the exclusive formation of the guest-exchange product $[\mathbf{M}\cdot\mathbf{H}\cdot\mathbf{B}]^+$ (Eqn 1). The pseudo-first-order rate constants k' of Eqn 1 were obtained from the slopes of the relevant $\ln(I/I_0)$ *vs.* t plots, where I is the signal intensity of the corresponding starting complex at the delay time t and I_0 is the sum of the signal intensities of the starting complex and its products. The second-order rate constants $k = k'/[\mathbf{B}]$, denoted according to the configuration of the host **M**, are listed in Table 1. Their values, compared with the relevant collision rate constant (k_C),[14] provide a measure of the percent efficiency of the reaction (eff $= 100k/k_C$). For the rate constants, k_{homo} refers to the complex where **A** and **M** have the "same" configuration (*i.e. R* for **1–5**) and k_{hetero} to that where **A** and **M** have the "opposite" configuration (*i.e. S* for **1–5**).

Enantioselectivity is defined by the $\rho = k_{homo}/k_{hetero}$ ratio. A $\rho > 1$ value indicates that the **B**-to-**A** displacement is faster in the homochiral complex than in the heterochiral one. The opposite is true when $\rho < 1$. A $\rho = 1$ value corresponds to equal displacement rates. Linear rate plots are invariably observed in the reaction of amine **B** with all the selected $[\mathbf{M}\cdot\mathbf{H}\cdot\mathbf{C}]^+$ complexes (corr. coeff. $0.990 < r^2 < 0.999$) and with $[\mathbf{M}\cdot\mathbf{H}\cdot\mathbf{V}]^+$ ($\mathbf{M} = \mathbf{1_{R/S}}$–$\mathbf{3_{R/S}}$; corr. coeff. $0.975 < r^2 < 1.000$). In contrast, bi-exponential kinetics are observed with $[\mathbf{4_{R/S}}\cdot\mathbf{H}\cdot\mathbf{V}]^+$. As pointed out in related studies,[7–9,15,16] this kinetic behaviour is ascribed to the occurrence of two stable isomeric $[\mathbf{4_{R/S}}\cdot\mathbf{H}\cdot\mathbf{V}]^+$ structures, one less reactive ($[\mathbf{4_{R/S}}\cdot\mathbf{H}\cdot\mathbf{V}]^+_{slow}$) and the other more reactive ($[\mathbf{4_{R/S}}\cdot\mathbf{H}\cdot\mathbf{V}]^+_{fast}$). The time dependence of $[\mathbf{4_{R/S}}\cdot\mathbf{H}\cdot\mathbf{V}]^+_{fast}$ (corr. coeff. $0.907 < r^2 < 0.975$) can be inferred from the overall $[\mathbf{4_{R/S}}\cdot\mathbf{H}\cdot\mathbf{V}]^+$ decay after subtracting the first-order decay of $[\mathbf{4_{R/S}}\cdot\mathbf{H}\cdot\mathbf{V}]^+_{slow}$ (corr. coeff. $0.983 < r^2 < 0.998$). The two

Table 1 Exchange rate constants ($k \times 10^{-11}$ cm^3 molecule^{-1} s^{-1})

Complex	(%)	k	$\rho = k_{homo}/k_{hetero}$	eff.[a] $= 100k/k_C$
$[\mathbf{1_R}\cdot\mathbf{H}\cdot\mathbf{C}]^+_{homo}$		1.11 ± 0.12	1.02 ± 0.14	0.9
$[\mathbf{1_S}\cdot\mathbf{H}\cdot\mathbf{C}]^+_{hetero}$		1.09 ± 0.10		0.9
$[\mathbf{2_R}\cdot\mathbf{H}\cdot\mathbf{C}]^+_{homo}$		8.04 ± 1.00	0.70 ± 0.14	6.9
$[\mathbf{2_S}\cdot\mathbf{H}\cdot\mathbf{C}]^+_{hetero}$		11.50 ± 1.80		9.9
$[\mathbf{3_R}\cdot\mathbf{H}\cdot\mathbf{C}]^+_{homo}$		1.91 ± 0.14	1.70 ± 0.22	1.6
$[\mathbf{3_S}\cdot\mathbf{H}\cdot\mathbf{C}]^+_{hetero}$		1.12 ± 0.12		1.0
$[\mathbf{4_R}\cdot\mathbf{H}\cdot\mathbf{C}]^+_{homo}$		2.37 ± 0.14	16.9 ± 2.8	2.0
$[\mathbf{4_S}\cdot\mathbf{H}\cdot\mathbf{C}]^+_{hetero}$		0.14 ± 0.02		0.1
$[\mathbf{5_R}\cdot\mathbf{H}\cdot\mathbf{C}]^+_{homo}$		0.88 ± 0.09	0.56 ± 0.07	0.7
$[\mathbf{5_S}\cdot\mathbf{H}\cdot\mathbf{C}]^+_{hetero}$		1.56 ± 0.12		1.3
$[\mathbf{1_R}\cdot\mathbf{H}\cdot\mathbf{V}]^+_{homo}$		0.54 ± 0.06	2.60 ± 0.38	0.5
$[\mathbf{1_S}\cdot\mathbf{H}\cdot\mathbf{V}]^+_{hetero}$		0.21 ± 0.02		0.2
$[\mathbf{2_R}\cdot\mathbf{H}\cdot\mathbf{V}]^+_{homo}$		1.68 ± 0.20	0.95 ± 0.16	1.5
$[\mathbf{2_S}\cdot\mathbf{H}\cdot\mathbf{V}]^+_{hetero}$		1.76 ± 0.20		1.4
$[\mathbf{3_R}\cdot\mathbf{H}\cdot\mathbf{V}]^+_{homo}$		0.52 ± 0.07	1.41 ± 0.24	0.4
$[\mathbf{3_S}\cdot\mathbf{H}\cdot\mathbf{V}]^+_{hetero}$		0.37 ± 0.04		0.3
$[\mathbf{4_R}\cdot\mathbf{H}\cdot\mathbf{V}]^+_{homo}$	*fast* (30)	4.57 ± 0.73	1.55 ± 0.27	3.9
$[\mathbf{4_S}\cdot\mathbf{H}\cdot\mathbf{V}]^+_{hetero}$	*fast*(37)	2.95 ± 0.21		2.5
$[\mathbf{4_R}\cdot\mathbf{H}\cdot\mathbf{V}]^+_{homo}$	*slow*(70)	0.21 ± 0.01	1.20 ± 0.09	0.2
$[\mathbf{4_S}\cdot\mathbf{H}\cdot\mathbf{V}]^+_{hetero}$	*slow*(63)	0.18 ± 0.01		0.1
$[\mathbf{5_R}\cdot\mathbf{H}\cdot\mathbf{V}]^+_{homo}$	k_2	1.39 ± 0.13	1.14 ± 0.17	1.0
$[\mathbf{5_S}\cdot\mathbf{H}\cdot\mathbf{V}]^+_{hetero}$	k_2	1.22 ± 0.14		1.2
$[\mathbf{5_R}\cdot\mathbf{H}\cdot\mathbf{V}]^+_{homo}$	k_{-2}[b]	0.061 ± 0.004	1.36 ± 0.15	
$[\mathbf{5_S}\cdot\mathbf{H}\cdot\mathbf{V}]^+_{hetero}$	k_{-2}[b]	0.045 ± 0.004		
$[\mathbf{5_R}\cdot\mathbf{H}\cdot\mathbf{V}]^+_{homo}$	k_1	0.57 ± 0.06	0.92 ± 0.12	0.5
$[\mathbf{5_S}\cdot\mathbf{H}\cdot\mathbf{V}]^+_{hetero}$	k_1	0.62 ± 0.05		0.5

[a] Reaction efficiency expressed by the percent ratio between the measured rate constants and the corresponding collision constant k_C, calculated using the trajectory calculation method (ref. 14); [b] k_{-2} in s^{-1}.

isomeric structures react with the amine **B** at rates differing by a factor ranging from *ca.* 16 to over 21. The Y-intercepts of the first-order decay of $[\mathbf{4}_{R/S}\cdot\mathbf{H}\cdot\mathbf{V}]^+_{slow}$ and $[\mathbf{4}_{R/S}\cdot\mathbf{H}\cdot\mathbf{V}]^+_{fast}$ provide an estimate of their relative distribution. The kinetic plots, described above, are reported in Figs S1–S9 of the Electronic Supplementary Information (ESI†) and the relevant results are in Table 1. With the diastereomeric $[\mathbf{5}_{R/S}\cdot\mathbf{H}\cdot\mathbf{V}]^+$ complexes, the displacement eqn 1 is accompanied by reversible **B** addition. The kinetic curves, shown in Figs S10–S11 of the ESI,† are consistent with Sequence 2. Best fitting of the relevant time-dependent ion abundances provides the k_x (x = 1, 2, and –2) values of Table 1.

$$\left[\mathbf{5}_{R/S}\bullet\mathrm{H}\bullet\mathrm{B}\right]^+ + \mathbf{V} \xleftarrow{k_1} \left[\mathbf{5}_{R/S}\bullet\mathrm{H}\bullet\mathbf{V}\right]^+ + \mathrm{B} \underset{k_2}{\overset{k_{-2}}{\rightleftarrows}} \left[\mathbf{5}_{R/S}\bullet\mathrm{H}\bullet\mathbf{V}\bullet\mathrm{B}\right]^+ \quad (2)$$

This kinetic scheme can be accounted for by a single stable $[\mathbf{5}_{R/S}\cdot\mathbf{H}\cdot\mathbf{V}]^+$ regioisomer which can accommodate the amine **B** on different regions of its structure. The competing occurrence of the reversible **B** addition to the complex (k_2 and k_{-2}) and of the direct guest displacement (k_1) requires different, not easily interchangeable points of attack of the **B** base on the $[\mathbf{5}_{R/S}\cdot\mathbf{H}\cdot\mathbf{V}]^+$ supramolecule. The scarce enantioselectivity of the displacement process (k_1; $\rho = 0.92 \pm 0.12$) suggests that vindoline in $[\mathbf{5}_{R/S}\cdot\mathbf{H}\cdot\mathbf{V}]^+$ is firmly located outside the cavity of the host in a position external to the chiral pendants. With this structural arrangement, the direct guest displacement (k_1), requiring the proton transfer from $\mathbf{V}H^+$ to **B**, may take place without any significant interactions of the two reactants with the chiral centres of the host. This structural arrangement may also account for the limited enantioselectivity of the reversible **B** association (k_2; $\rho = 1.14 \pm 0.17$ and k_{-2}; $\rho = 1.36 \pm 0.15$) probably involving the incorporation of the amine inside the chiral host cavity.

According to the ρ ratios of Table 1, the $[\mathbf{4}_{R/S}\cdot\mathbf{H}\cdot\mathbf{C}]^+$ complexes show the greatest enantioselectivity with the homochiral complex reacting *ca.* 17 times faster than the heterochiral one. The same trend, though much less evident, is observed with the $[\mathbf{3}_{R/S}\cdot\mathbf{H}\cdot\mathbf{C}]^+$ adducts. The homochiral adduct reacts only *ca.* 1.7 times faster than the heterochiral one. The opposite selectivity is observed with the $[\mathbf{2}_{R/S}\cdot\mathbf{H}\cdot\mathbf{C}]^+$ and $[\mathbf{5}_{R/S}\cdot\mathbf{H}\cdot\mathbf{C}]^+$ complexes ($\rho < 1$), whereas the $[\mathbf{1}_{R/S}\cdot\mathbf{H}\cdot\mathbf{C}]^+$ adducts do not display any significant enantioselectivity ($\rho = 1$). Thus, replacement of the COOMe ends of the host pendants in $[\mathbf{1}_{R/S}\cdot\mathbf{H}\cdot\mathbf{C}]^+$ with the COOH functionality (as in $[\mathbf{2}_{R/S}\cdot\mathbf{H}\cdot\mathbf{C}]^+$) induces an appreciable enantioselectivity in the **B**-to-**C** displacement process. Besides, comparison of eqn 1 kinetics for $[\mathbf{1}_{R/S}\cdot\mathbf{H}\cdot\mathbf{C}]^+$ and $[\mathbf{3}_{R/S}\cdot\mathbf{H}\cdot\mathbf{C}]^+$ reveals that inverting the amino acid sequence in the host pendants from *val-leu* ($[\mathbf{1}_{R/S}\cdot\mathbf{H}\cdot\mathbf{C}]^+$) to *leu-val* ($[\mathbf{3}_{R/S}\cdot\mathbf{H}\cdot\mathbf{C}]^+$) enhances the rate constant of the homochiral complex while that of the heterochiral one remains essentially constant.

Eqn 1 on the selected $[\mathbf{M}\cdot\mathbf{H}\cdot\mathbf{V}]^+$ complexes exhibits an enantioselectivity which somewhat parallels that shown by the corresponding $[\mathbf{M}\cdot\mathbf{H}\cdot\mathbf{C}]^+$ adduct. Thus, both $[\mathbf{3}_{R/S}\cdot\mathbf{H}\cdot\mathbf{V}]^+$ and $[\mathbf{4}_{R/S}\cdot\mathbf{H}\cdot\mathbf{V}]^+$ complexes display a ρ value greater than 1, which indicates that the corresponding homochiral forms react faster than the heterochiral ones. The same applies to the $[\mathbf{1}_{R/S}\cdot\mathbf{H}\cdot\mathbf{V}]^+$ complexes, whereas, as mentioned above, the $[\mathbf{5}_{R/S}\cdot\mathbf{H}\cdot\mathbf{V}]^+$ ones do not exhibit any significant enantioselectivity (k_1, k_2, and k_{-2}; $\rho \geq 1$). Contrary to $[\mathbf{2}_{R/S}\cdot\mathbf{H}\cdot\mathbf{C}]^+$, the replacement of the COOMe ends of the host pendants in $[\mathbf{1}_{R/S}\cdot\mathbf{H}\cdot\mathbf{V}]^+$ ($\rho > 1$) with the COOH functionality (as in $[\mathbf{2}_{R/S}\cdot\mathbf{H}\cdot\mathbf{V}]^+$) makes the **B**-to-**V** displacement process unselective ($\rho = 1$). Differently from the corresponding complexes with **C**, comparison of the kinetics of eqn 1 for $[\mathbf{1}_{R/S}\cdot\mathbf{H}\cdot\mathbf{V}]^+$ and $[\mathbf{3}_{R/S}\cdot\mathbf{H}\cdot\mathbf{V}]^+$ reveals that, in this case, inverting the amino acid sequence in the host pendants from *val-leu* ($[\mathbf{1}_{R/S}\cdot\mathbf{H}\cdot\mathbf{V}]^+$) to *leu-val* ($[\mathbf{3}_{R/S}\cdot\mathbf{H}\cdot\mathbf{V}]^+$) enhances the rate constant of the heterochiral complex while that of the homochiral one remains essentially constant.

Given the exceptional molecular complexity of all the selected $[\mathbf{M}\cdot\mathbf{H}\cdot\mathbf{A}]^+$ complexes and in consideration of the fact that only in a few cases the ρ factors of Table 1 diverge significantly from unity, any attempt to provide an unequivocal rationale for all the observed enantioselectivities may appear foolishly ambitious and unlikely to be definitive. In fact, small deviations of ρ from unity may be accounted for by kinetic factors, *i.e.* related to the effects of the **M** host chiral frame upon the eqn 1 transition structures, and/or by thermodynamic factors, *i.e.* just reflecting the relative stability of the diastereomeric $[\mathbf{M}\cdot\mathbf{H}\cdot\mathbf{A}]^+$ complexes. For these reasons, we focussed our attention on the diastereomeric $[\mathbf{4}_{R/S}\cdot\mathbf{H}\cdot\mathbf{C}]^+$ complexes which display such an exceptional enantioselectivity ($\rho = 16.9 \pm 2.8$) that this must reflect large differences in the relevant eqn 1 coordinate. To elucidate these differences, detailed structural and energetic analyses of catharanthine (**C**), its N(6)-protonated derivative ($\mathbf{C}H^+$), and its diastereomeric $[\mathbf{4}_{R/S}\cdot\mathbf{H}\cdot\mathbf{C}]^+$ complexes have been undertaken by using molecular mechanics (MM) calculations and molecular dynamics (MD) simulations.

Conformational study on C and CH^+

MM calculations and MD simulations on the **C** molecule were first performed in vacuum. A quite narrow spectrum of 14 low-energy stable conformers was found within 3 kcal mol^{-1} above the global minimum. The conformations populated at room temperature, according to the Boltzmann distribution, were filtered to afford two families of conformers. The two families are named according to the conformation of the seven-membered ring adjacent to the indole moiety of **C**. Thus, the most stable family is named *skew-boat* and the less stable one *chair* (Chart 3). The *skew-boat* conformation is the global minimum geometry of **C** and is about 1 kcal mol^{-1} more stable than the *chair* conformation. Other minima of each family, populated at room temperature, differ from their low-energy parent geometry in the orientation of the C(4)-Et and C(18)-COOMe side chain of the compound. Concerning the latter, only two orientations resulted in being allowed. In the *skew-boat* conformation, where the C(18)-COOMe bond is almost perpendicular to the indole plane, the carbonyl group of COOMe is oriented *syn* to the indolic NH moiety (orientation henceforth denoted as 0°) or *anti* to the same group (orientation henceforth denoted as 180°). The orientation of the indole moiety affected the conformation of the seven-membered ring so that

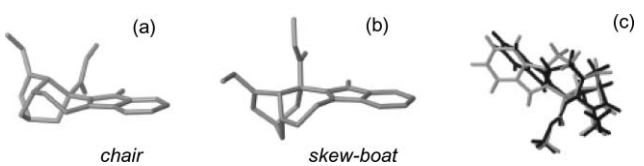

Chart 3 Most stable conformations of (+)-catharanthine **C**: (a) *chair*; (b) *skew-boat*. Figure (c) shows the superimposition between the *chair* (gray) and the *skew-boat* (black) conformational minima of (+)-catharanthine (**C**).

a 40° counterclockwise rotation of this system around the bond connecting it to the quaternary bridge carbon atom brings it from the *skew-boat* to the *chair* geometry (Chart 3c).

A conformational search of N(6)-protonated catharanthine (**C**H$^+$) was performed in a vacuum as well as in generalized born/solvent accessible (GB/SA) implicit water to investigate the effect of the physical environment on the conformational preferences of the molecule. As expected, no crucial differences in geometries and intramolecular energy contributions came out with respect to the search performed for neutral **C** in a vacuum: 11 minima were detected within 3 kcal mol^{-1} above the global minimum. Again, the *skew-boat* form was the global minimum.

The only aspect deserving attention was that solvation and torsional energy terms favour the *chair* conformation with respect to *skew-boat* one by several hundreds calories per mol, while the electrostatic contribution largely advantages the global minimum conformation and settles the steric energy rankings (results not shown).

MD simulations were performed both in a vacuum and in GB/SA implicit water to investigate the conformational behaviour of both **C** and **C**H$^+$ at room temperature in different physical environments. A vacuum was chosen as an ideal extreme condition of no solvation to maximise the effect of intramolecular noncovalent interactions on flexibility. In contrast, in water, intermolecular interactions with the solvent are expected to shield intramolecular effects. Simulations lasting 20 ps were performed selecting a few low-energy minima, including *skew-boat* and *chair*, as input structures. The results of the runs are summarised in Fig. 1–4. Fig. 1 refers to neutral **C** in a vacuum (MD simulations performed on **C** in GB/SA implicit water did not modify appreciably the picture emerging from the graphs displayed in the figure) and shows respectively: a) the time evolution in a vacuum of the dihedral angle centred on the bond connecting the two CH_2 groups of the seven member ring (ethylene dihedral); b) the time evolution in a vacuum of the dihedral angle centred on the bond connecting the ester group to the seven member ring (ester dihedral); c) the time evolution of the dihedral angle centred on the bond connecting the ethyl group to the cyclohexene ring (ethyl dihedral). The runs concerning **C**H$^+$ in a vacuum and in GB/SA implicit water are illustrated in Fig. 2 and Fig. 3–4, respectively.

All the runs indicate that the *skew-boat* structure of both **C** and **C**H$^+$ is persistent throughout (Fig. 1a and 2a). A run performed on **C**H$^+$ in water (Fig. 3a and 4a) highlighted a facile interconversion of the *chair* geometry into the *skew-boat* conformation. In all simulations, the ethyl substituent was free to move in 3D space (Fig. 1c–4c). The ester group changed from a 0° to a 180° orientation and *vice versa*, many times (Fig. 1b, 3b, and 4b), except for in **C**H$^+$ in a vacuum where its carbonyl group remained *anti* to the indole NH (Fig. 2b).

When all the information was put together, a picture of the conformational behaviour of **C** and **C**H$^+$ emerges. These compounds have structures with condensed six- and seven-membered rings and are characterised by the proximity in 3D space of two polar groups, *i.e.* COOMe and the indole NH, which can favourably interact each other. Three major contributions to the molecular energy compete with each other to settle the *skew-boat vs. chair* conformational ranking in **C** and **C**H$^+$, namely electrostatic, torsion, and solvation energies. Torsion and solvation energies favour the *chair* geometry, whereas electrostatic energy favours

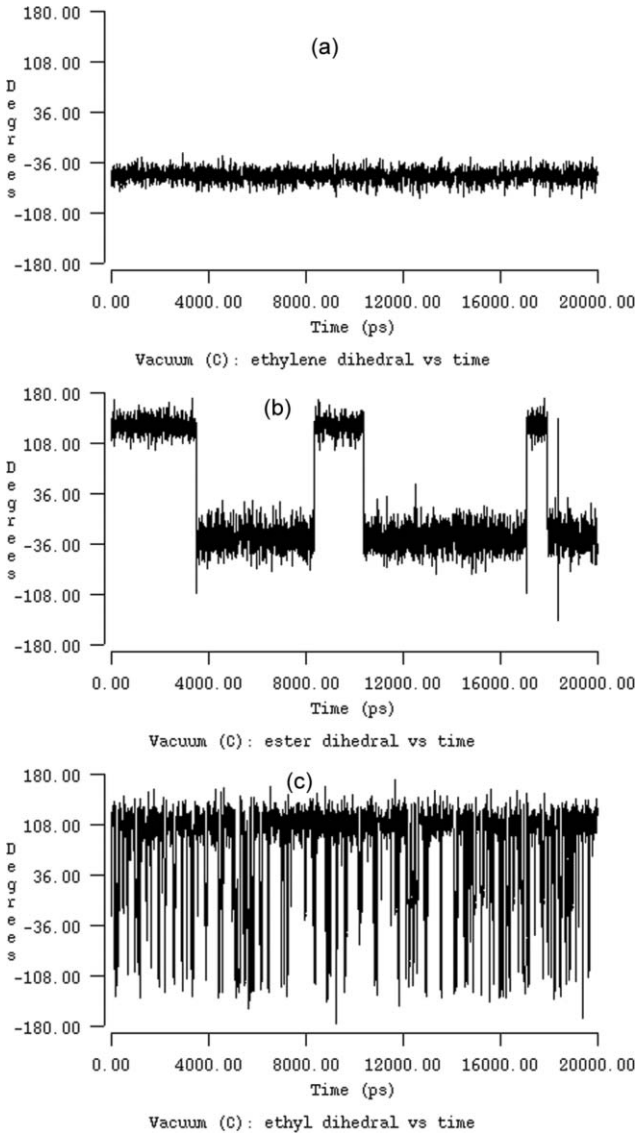

Fig. 1 Neutral **C** in a vacuum: a) time evolution of the ethylene dihedral; b) time evolution of the ester dihedral; c) time evolution of the ethyl dihedral.

the *skew-boat* one. The favourable torsional contribution to *chair* geometry is not surprising since it corresponds to the general expectations on the energy ranking of seven-membered rings. Repulsive electrostatic interactions between the indole NH and ester CO dipoles appear to be less effective in the *skew-boat* than in the *chair* geometry to the point of overwhelming all the other effects. Indeed, in a medium with a low dielectric constant (vacuum), electrostatic interactions dominate so that the **C** molecule, and the **C**H$^+$ ion even more, are locked in the *skew-boat* conformations by inhibiting their conversion to the *chair* ones. In a medium with high dielectric constant (water), intramolecular electrostatic interactions are abated by multiple effective interactions between **C**H$^+$ and the polar solvent. In this medium, torsional and solvation factors might become comparable to intramolecular electrostatic factors and, consequently, the conformational flexibility of the structure might increase. Precious experimental support for the results of the MD simulations was found from detailed NMR

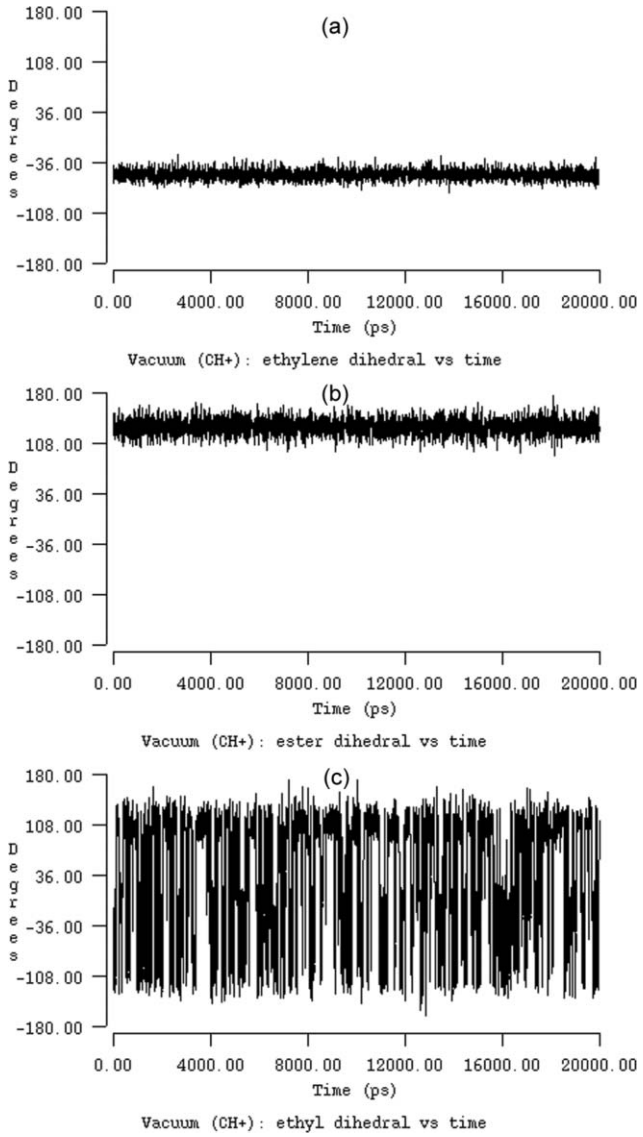

Fig. 2 Protonated catharanthine **C**H$^+$ in a vacuum: a) time evolution of the ethylene dihedral; b) time evolution of the ester dihedral; c) time evolution of the ethyl dihedral.

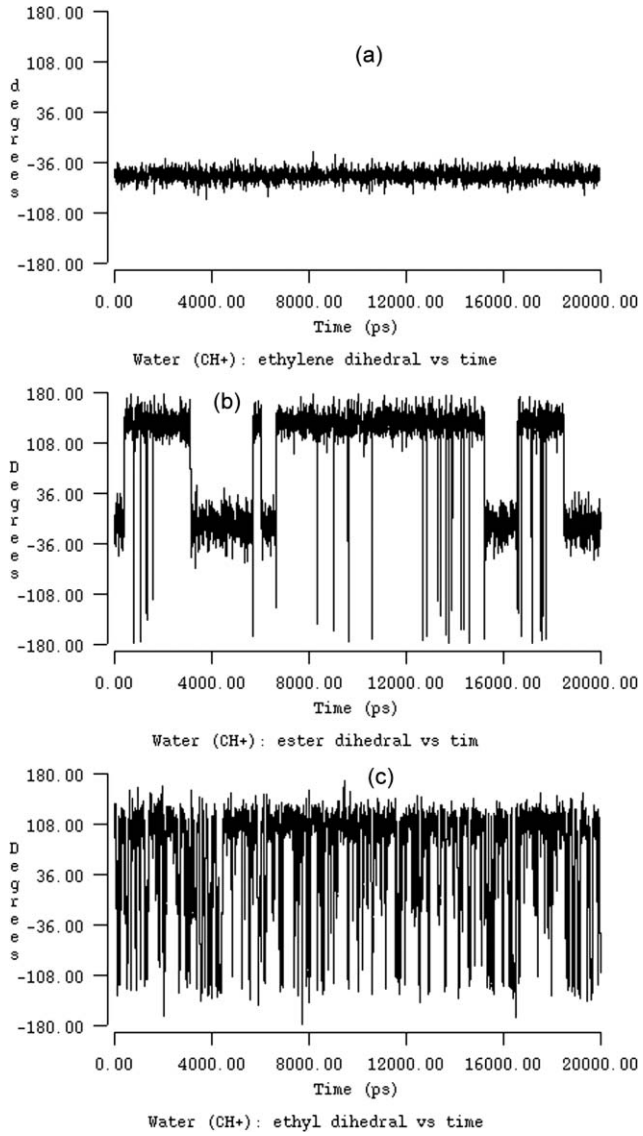

Fig. 3 Protonated catharanthine **C**H$^+$ ("*skew-boat* conformation") in GB/SA implicit water: a) time evolution of the ethylene dihedral; b) time evolution of the ester dihedral; c) time evolution of the ethyl dihedral.

analysis of the **C** molecule in an apolar solvent, like CH_2Cl_2, and of the **C**H$^+$ ion in water.

NMR experiments

The ^{1}H spectrum of **C** in CD_2Cl_2 (Fig. 5a) is well resolved with sharp signals suggesting a single predominant conformation or several conformers rapidly interconverting relative to the NMR timescale. The corresponding assignments obtained by 2D NMR experiments are reported in the ESI.† In order to investigate the effect of protonation, a small amount of **C** was dissolved in D_2O, at different pH. The ^{1}H spectra of **C** at pH = 10.8 (Fig. 5b) and **C**H$^+$ at pH = 5.4 (Fig. 5c) appear well resolved with sharp signals suggesting again either a single predominant conformation or fast interconverting conformers.

Note the significant variation in chemical shifts of groups in the neighbourhood of the protonation site in the **C**H$^+$ spectrum. Note also that ^{1}H NMR spectra of **C** at pH values intermediate between 10.8 and 5.4 show an exchange broadening of the resonances due to C(8)H_2, C(7)H_2 and C(19)H_2 groups in the neighbourhood of the site of protonation (Fig. 5d). Taking into account the results of the MD simulations, described in the previous Section, the sharp signals, observed in Fig. 5a–c, can be attributed to either **C** (Fig. 5a–b) or **C**H$^+$ (Fig. 5c) in the predominant *skew-boat* conformation. The signal broadening, observed in D_2O at 10.8 > pH > 5.4, is attributable to a relatively slow proton transfer between coexisting *skew-boat* **C** and *skew-boat* **C**H$^+$.

Concerning the conceivable occurrence of the [$\mathbf{4}_{R/S}$·**H**·**C**]$^+$ complexes in liquid media, the NMR technique is generally considered as a power tool for the study of noncovalent interactions in diastereomeric host/guest complexes in solution.[17] The occurrence of diastereomeric complexes, like [$\mathbf{4}_{R/S}$·**H**·**C**]$^+$, is usually evidenced by the chemical shift non-equivalence of the signals from the two diastereomeric complexes. The success of the NMR investigation depends on many factors, such as the structural features of the

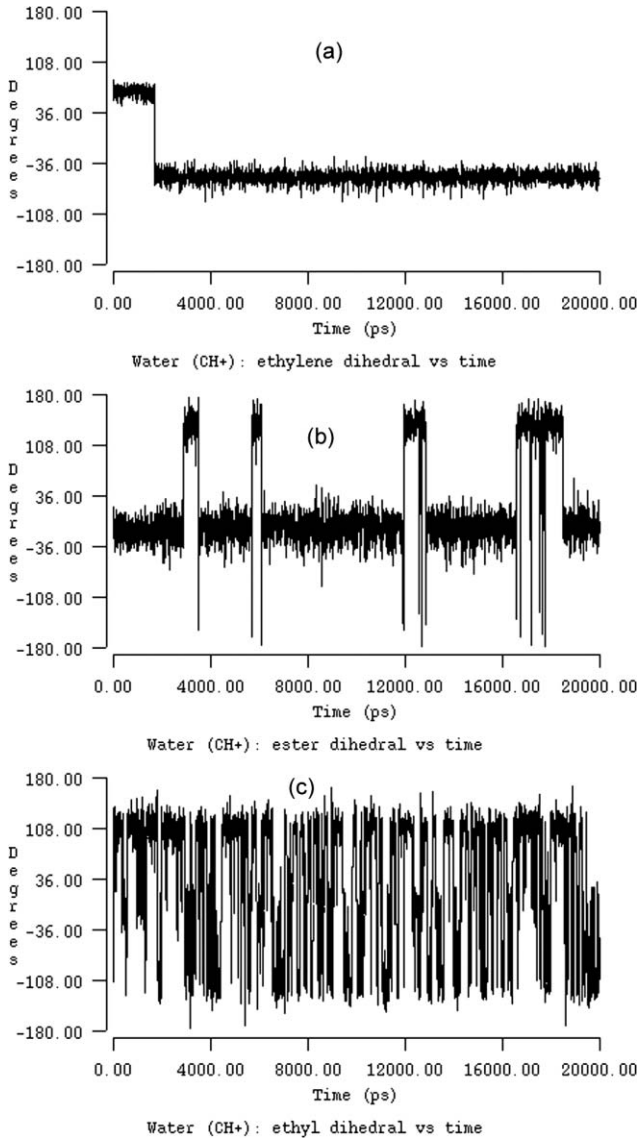

Fig. 4 Protonated catharanthine **C**H$^+$ ("*chair* conformation") in GB/SA implicit water: a) time evolution of the ethylene dihedral; b) time evolution of the ester dihedral; c) time evolution of the ethyl dihedral.

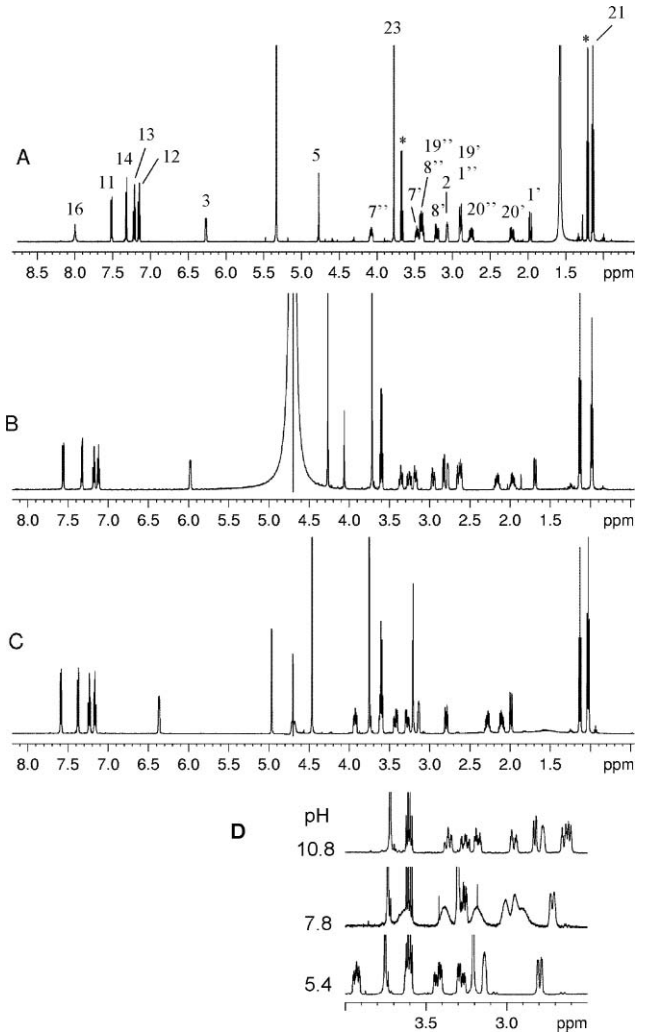

Fig. 5 ^{1}H 600.13 MHz spectra of : (A) **C** in CD_2Cl_2; (B) **C** in D_2O at pH = 10.8; (C) **C**H$^+$ in D_2O at pH = 5.4. For the assignments, see ESI† and for the numbering, Chart 1; (*) ethanol. Inset (D): ^{1}H spectra (middle field region) of **C** in D_2O at different pH showing the broadening of the $C(8)H_2$, $C(7)H_2$ and $C(19)H_2$ signals at $5.4 < pH < 10.8$.

host and the guest, their solubility in a given solvent, and so on. Therefore, we tried to study the interaction of **C** with the $\mathbf{4}_{R/S}$ enantiomers both in CD_2Cl_2 and in D_2O. In CD_2Cl_2, both **C** and $\mathbf{4}_{R/S}$ are soluble and the spectrum of their mixture did not show any evidence of interactions. In D_2O, instead, $\mathbf{4}_{R/S}$ is almost completely insoluble and the ^{1}H spectrum of its saturated mixture with **C** did not show any signals of the amido[4]resorcinarene, even two weeks after sample preparation. Therefore, some information on the structure and the dynamics of $[\mathbf{4}_{R/S}\cdot\mathbf{H}\cdot\mathbf{C}]^+$ can be obtained only by resorting to MM calculations and MD simulations.

MM and MD calculations on diastereomeric $[\mathbf{4}_{R/S}\cdot\mathbf{H}\cdot\mathbf{C}]^+$ complexes

Docking studies were performed first[18] in the gas phase to detect the three dimensional structure of both complexes in the absence of thermal motion (0 K temperature). All calculations converge unambiguously towards two particular lowest energy geometries (one for the heterochiral complex and one for the homochiral one), showing a different recognition of the guest compound in the *skew-boat* conformation by the two chiral hosts.

Fig. 6b,c, depict the two global minima as found by MCMM/MOLS docking simulations on the heterochiral $[\mathbf{4}_S\cdot\mathbf{H}\cdot\mathbf{C}]^+$ and on the homochiral $[\mathbf{4}_R\cdot\mathbf{H}\cdot\mathbf{C}]^+$ complexes, respectively. Several structural features are shared by the two global minima. First of all, to accommodate the *skew-boat* catharanthine, both host enantiomers have to heavily adjust their structures with respect to their gas phase uncomplexed global minima.[6] The intramolecular hydrogen bonding network at the lower rim is modified considerably to let a couple of adjacent carbonyl oxygen atoms be directed towards the guest. Notably, such a pre-organisation produces two mirror-image asymmetric hosting areas (Fig. 6a). Moreover, protonated *skew-boat* catharanthine looks to be invariantly located at the lower rim of the host, in front of one of the two facing vertical aromatic rings, with the protonated

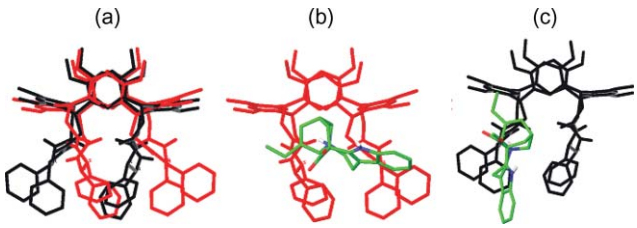

Fig. 6 Monte Carlo global minimum geometry of the $[\mathbf{4}_S\cdot\mathbf{H}\cdot\mathbf{C}]^+$ (b) and $[\mathbf{4}_R\cdot\mathbf{H}\cdot\mathbf{C}]^+$ (c) complexes, showing the preferred accommodation of the **C** guest (green in (b) and (c)) outside the host cavity among the two chiral pendants. Figure (a) shows the superimposition between the geometries of compound $\mathbf{4}_S$ (red) and $\mathbf{4}_R$ (black), as found in the docking global minimum energy complexes.

nitrogen forming one hydrogen bonding interaction (not shown in the figure) with one of the two carbonyl groups of the host. Despite the abovementioned similarities, the orientation of catharanthine seems to be markedly different in the two complexes (Fig. 6b,c) due to the asymmetry of the hosting area. Even taking into account all the low energy minima of each complex, collected within 5 kcal mol^{-1} energy windows over the global minimum, it results that the *skew-boat* catharanthine is accommodated differently in the heterochiral $[\mathbf{4}_S\cdot\mathbf{H}\cdot\mathbf{C}]^+$ and in the homochiral $[\mathbf{4}_R\cdot\mathbf{H}\cdot\mathbf{C}]^+$ complexes (Fig. S12 of the ESI†).

MD simulations were performed at 300 K starting from all the minima discussed above. They did not show any conformational/configurational interconversion during the runs and allowed comparison between the average enthalpies of the corresponding complexes at room temperature. The global minimum complexes showed enthalpy values differing by roughly 1–2 kcal mol^{-1} in favour of the homochiral one *which is the more reactive diastereoisomer towards* ***B***. This observation excludes that the selectivity of the diastereomeric $[\mathbf{4}_{R/S}\cdot\mathbf{H}\cdot\mathbf{C}]^+$ complexes towards **B**, measured in the FT-ICR-MS experiments, is simply due to the difference in their thermodynamic stability. Rather, a more plausible rationale for the greater enantioselectivity of eqn 1 can arise from the observation that the hosts in the diastereomeric $[\mathbf{4}_{R/S}\cdot\mathbf{H}\cdot\mathbf{C}]^+$ complexes present mirror-image asymmetric cavities wherein the chiral guest is differently oriented and leaves more or less space for the access of **B** into the cavities themselves (Fig. 6 and Fig. S12 of the ESI†). Indeed, the occurrence of displacement eqn 1 requires $[\mathbf{C}H^+\cdots O{=}C\text{-host}] + \mathbf{B} \rightarrow [\mathbf{B}\cdots H^+O{=}C\text{-host}] + \mathbf{C}$ proton transfer in the proximity of the host cavity. In the absence of the guest, the access of amine **B** into the mirror-image asymmetric cavities of the host in the diastereomeric $[\mathbf{4}_{R/S}\cdot\mathbf{H}\cdot\mathbf{C}]^+$ complexes would be almost equally probable.[19] However, this is no longer true in the presence of the chiral guest. According to the structures shown in Fig. 6 and Fig. S12 of the ESI,† the much greater efficiency of eqn 1, measured for the homochiral $[\mathbf{4}_R\cdot\mathbf{H}\cdot\mathbf{C}]^+$ complex, can be accounted for by the larger local concentration of **B** determined by its easier access to the host cavity. In other words, the exceptional enantioselectivity ($\rho = 16.9 \pm 2.8$) exhibited by the diastereomeric $[\mathbf{4}_{R/S}\cdot\mathbf{H}\cdot\mathbf{C}]^+$ complexes in eqn 1 is due to kinetic factors. Whether this large ρ value is determined only by the relevant pre-exponential terms or by the different stability of the corresponding transition structures as well is still open to question.

Comparison with biochemical studies

Previous comprehensive biochemical studies have shown that, of the two moieties of vinblastine, *i.e.* (+)-catharanthine (**CC**) and (–)-vindoline (**V**), **C** is vastly more active than **V** by itself in inhibiting the self-assembly of tubulin into microtubules and in inducing the polymerization of tubulin into linear structures.[20] The presence of a covalent linkage between **C** and **V** in vinblastine enhances its binding to tubulin by orders of magnitude relative to that of the separated **C** and **V** molecules, though part of the association free energy in vinblastine is spent in freezing the free rotations between the two moieties and inducing strain by complexation with tubulin molecules. (+)-Catharanthine (**C**) induces the same self-assembly process of vinblastine. A similar correspondence cannot be established for **V** whose role is thought to be simply the anchoring of the bidentate ligand. This means that **C** contains the structural requisites for inducing in tubulin the conformational state essential for the protein to self-assemble into linear structures. Such structural features can be determined by comparing the structures of the **C** molecule and its modified counterpart when incorporated into vinblastine. The two are identical only in the indole part and in the C(8)-C(7)-N(6) portion of the polycyclic ring, namely the side chain mostly involved in the *skew-boat* ⇆ *chair* conformational equilibrium in the **C** molecule.

The results of MM and MD calculations on diastereomeric $[\mathbf{4}_{R/S}\cdot\mathbf{H}\cdot\mathbf{C}]^+$ complexes point to $\mathbf{C}H^+$ in the *skew-boat* conformation placed in front of one of the two facing vertical aromatic rings, with the protonated N(6) nitrogen H-bonded to one of the two carbonyl groups of the host. The same model may account for the binding of vinblastine to tubulin taking place in two consecutive steps involving a rapid equilibrium collision complex followed by a slower rearrangement inducing structural changes in the tubulin heterodimers. Each of the vinblastine subunits **C** and **V** interacts with both tubulin subunits α2 and β1 to approximately the same extent. In the presence of the drug, the side-chain of the acidic Aspβ179 residue moves to the vicinity of **C**, thus reproducing a sort of preliminary $N(6)\text{-}H^+\cdots{}^-O{=}C$-residue electrostatic interaction. This interaction is accompanied by extensive conformational modification of both α2 and β1 tubulin subunits as it happens with the $\mathbf{4}_{R/S}$ hosts. On one side, these conformational changes inhibit the activity of the β1 subunit and, on the other, allow reorientation of several α2 residues so as to establish intracomplex contacts stabilising curved protofilaments leading to spiral-like tubulin aggregates.

Conclusions

The structure and the favoured conformation of (+)-catharanthine (**C**), the constituent together with (–)-vindoline (**V**) of vincristine and vinblastine, have been investigated in different physical environments by combined experimental and computational methodologies. (+)-Catharanthine (**C**) and its N(6)-protonated form $\mathbf{C}H^+$ exhibit a stable *skew-boat* conformation in a vacuum and in water, as well as when interacting with the chiral amido[4]resorcinarene receptors **M** = **1**–**5**. The gas phase kinetics and enantioselectivity of the base-induced displacement reaction between (*R*)-(–)-2-butylamine (**B**) and the diastereomeric $[\mathbf{M}\cdot\mathbf{H}\cdot\mathbf{C}]^+$ and $[\mathbf{M}\cdot\mathbf{H}\cdot\mathbf{V}]^+$ complexes are mainly determined by the nature and the isomeric structure of the host's asymmetric pendants. MD simulations

indicate that the diastereomeric $[\mathbf{4}_{R/S}\cdot\mathbf{H}\cdot\mathbf{C}]^+$ complexes are quasi-degenerate, thus suggesting that the pronounced enantioselectivity of the base-induced **C** displacement reaction ($\rho = 16.9 \pm 2.8$) is mostly due to kinetic factors. The present kinetic, spectroscopic, and dynamic study of tailor-made simplified models may be considered as a starting point for a deeper comprehension of the intrinsic factors that endow **C** and **V**, and their dimeric forms, with their corresponding anticancer activity.

Experimental section

Materials

Enantiomerically pure **M** = **1–5**, in their flattened-cone conformation, were synthesised and purified according to established procedures.[6] (+)-Catharanthine (**C**) and (–)-vindoline (**V**) were purchased from a commercial source and used without further purification. The same source provided the (*R*)-(–)-2-butylamine (**B**), which was degassed in the vacuum manifold with several freeze–thaw cycles.

FT-ICR-MS experiments

The experiments were carried out with an APEX III (7T Magnet) FT-ICR-MS equipped with an Apollo ESI source (Bruker Daltonik GmbH, Bremen). Stock H_2O/CH_3OH= 1:3 solutions of $\mathbf{M} = \mathbf{1}_{R/S}$–$\mathbf{5}_{R/S}$ (1×10^{-5} M), containing a five-fold excess of **A** = (+)-catharanthine (**C**) or (–)-vindoline (**V**) were electrosprayed through a heated capillary ($T = 130$ °C) into the external source of the FT-ICR mass spectrometer. The resulting ions were transferred into the resonance cell by a system of potentials and lenses and quenched by collisions with argon pulsed into the cell through a magnetic valve. ESI of **M**/**A** solutions leads to the formation of abundant signals, corresponding to the natural isotopomers of the proton-bound complex $[\mathbf{M}\cdot\mathbf{H}\cdot\mathbf{A}]^+$, which were monitored and isolated by broad-band ejection of the accompanying ions. The isolated $[\mathbf{M}\cdot\mathbf{H}\cdot\mathbf{A}]^+$ complex was allowed to react with the chiral amine **B** present in the cell at a fixed concentration whose value ranges from 1.2×10^9 to 7.8×10^9 molecule cm^{-3} depending upon its reactivity.

NMR experiments

NMR spectra were recorded on a Bruker AVANCE AQS600 spectrometer operating at the proton frequency of 600.13 MHz and equipped with a Bruker multinuclear *z*-gradient inverse probe head capable of producing gradients in the *z* direction with a strength of 55 G cm^{-1}. ^{1}H and ^{13}C NMR spectra of **C** in CD_2Cl_2 were referenced with respect to the residual proton signal of $CHDCl_2$ ($\delta = 5.33$ ppm) and to the carbon signal of CD_2Cl_2 at ($\delta = 54.2$ ppm), respectively. ^{1}H and ^{13}C NMR spectra of **C** in D_2O were referenced with respect to ^{1}H and ^{13}C signals of ethanol present as an impurity ($\delta_H = 1.131$ ppm and $\delta_C = 17.1$ ppm). 1D experiments in D_2O were acquired using low-power presaturation of the HDO signal.[21]

2D ^{1}H-^{1}H COSY, ^{1}H-^{1}H TOCSY, ^{1}H-^{1}H NOESY ^{1}H-^{13}C HSQC, ^{1}H-^{13}C HMBC experiments were recorded using a recycle delay of 2 s, 1 k data points in f2 dimension, and 512 increments in f1 dimension. ^{1}H-^{1}H COSY were acquired in magnitude mode whilst ^{1}H-^{1}H TOCSY experiments with a contact time of 80 ms and ^{1}H-^{1}H NOESY experiments with a mixing time of 400 ms were both acquired in phase-sensitive mode using TPPI selection.

^{1}H-^{13}C Gradient-selected HSQC experiments with GARP decoupling were acquired in phase-sensitive mode using echo-antiecho selection optimized on 150 Hz; ^{1}H-^{13}C gradient-selected HMBC were recorded in magnitude mode and optimised for a one-bond coupling of 140 Hz and long-range couplings of 62.5 Hz.

Computational details

All the computational calculations were carried out and visualized on Intel Linux PCs incorporating Pentium IV CPUs.

MM calculations (docking) and MD simulations (MD) were performed using the AMBER* force field as implemented in MacroModel 8.6 and 9.0. The Maestro GUI was used as an interface to MacroModel. No cutoff was applied for the non-bonded interactions and the calculations were performed in the gas phase selecting the constant dielectric treatment (dielectric constant $\varepsilon = 1.0$). RESP partial atomic charges[22] of $\mathbf{4}_{R/S}$, to be used in the docking and MD simulations had been already calculated[6] and were used in this study without any modification. In the case of **C** and **C**H$^+$, RESP charges were calculated on the entire molecular structures by application of a protocol recently described.[18] The partial atomic charges are specified in the last column of the cartesian coordinate structures in the ESI† (mol2 format).

Insights into the structure and the dynamics of catharanthine and of the proton-bound $[\mathbf{4}_{R/S}\cdot\mathbf{H}\cdot\mathbf{C}]^+$ complexes were obtained by using two computational methodologies implemented in MacroModel, that is i) the statistical conformational search/docking procedure Monte Carlo Multiple Minimum (MCMM)[5] and ii) constant temperature MD runs. Each MCMM conformational search on catharanthine was started after having performed the MacroModel automatic setup to set all the search variables (torsions to be rotated, rings to be opened, *etc.*). Summing up, 3000 steps were invariably performed each time, in which a total number of 11 torsional degrees of freedom was analysed. A randomly variable number of rotatable bonds of the molecules ranging from 2 to 10 was varied in each step in the range 0°–180°. Three bonds within the three rings of catharanthine were temporarily broken to sever the rings for the purpose of Monte Carlo torsion angle searching and, after that, closed again with a minimum and maximum allowable ring closure distance of 0.5 and 2.5 Å, respectively. Energy minimizations were performed using the Polak Ribiere conjugate gradient (PRCG) procedure and were terminated when the energy gradient root mean square (rms) fell below 2.4 cal mol^{-1} Å^{-1}. A comparison was performed among the heavy atoms of the output structures to eliminate duplicate conformations, selecting 1.0 Å as the maximum allowable separation between couples of corresponding atoms after superimposition. All the unique conformers were saved that differed from the global minimum-energy conformation by less than 5 kcal mol^{-1}.

In the case of the Monte Carlo dockings, the conformational analysis of the two interacting partners was coupled with random rototranslations (MOLS command) of the guest species (**C**H$^+$) relative to the host ($\mathbf{4}_{R/S}$) standing still in 3D space (MCMM/MOLS docking). Each MCMM/MOLS run was made of 5000 steps. The rototranslations of the protonated guest were limited by the

maximum values of 180° for the rotational angle and of 5 Å for the translational movement. The flexibility of the resorcarene skeleton was not directly sampled, while only the seven-membered ring (see above) and the two side chains of catharanthine were randomly varied. A total number of 17 torsional degrees of freedom was analysed (14 belonging to the host compound's cyclic pendants and 3 to the guest). Two bonds within the cyclic pendants of $\mathbf{4}_{R/S}$ were temporarily broken to sever the rings for the purpose of Monte Carlo torsion angle searching and, after that, closed again with a minimum and maximum allowable ring closure distance of 0.5 and 3.5 Å, respectively. A randomly variable number of rotatable bonds ranging from 2 to 16 was varied in each step in the range 0°–180°. Energy minimisations were performed using the PRCG procedure and were terminated when the energy gradient root mean square (rms) fell below 2.4 cal mol^{-1} $Å^{-1}$. A comparison was performed among the heavy atoms of the output structures to eliminate duplicate conformations, selecting 1.2 Å as the maximum allowable separation between couples of corresponding atoms after superimposition. All the unique conformers were saved that differed from the global minimum-energy conformation by less than 5 kcal mol^{-1}.

Constant temperature MD simulations with generation of the canonical ensemble were performed at 300 K with a time step of 1.0 fs. The SHAKE algorithm was not applied. Coupling between the temperature bath and the molecules was updated every 0.2 ps. The equilibration period was 500 ps for every run, while the total simulation time was 20 ns. During each trajectory, 5000 structures (frames) were sampled at regular intervals throughout the time course. Each simulation (both conformational searching and molecular dynamics) was repeated a few times starting from different arbitrary geometries to produce a complete sampling of the whole potential energy hypersurface of the selected $[\mathbf{4}_{R/S}\cdot\mathbf{H}\cdot\mathbf{C}]^+$ systems. The convergence of the results guaranteed the completeness of the analysis.

Acknowledgements

Work was supported by the Ministero dell'Istruzione dell'Università e della Ricerca (MIUR). Financial support by Università "Sapienza", Roma, Italy (Funds for selected research topics 2008–2010), FIRST grant no. RBIP067F9E, FIRB grant no. RBPR05NWWC_006, and PRIN grant no. 2007H9S8SW_002 are acknowledged. JM and MCL also gratefully acknowledge financial support by the Deutsche Forschungsgemeinschaft (SFB 613).

References

1 N. Neuss, M. N. Neuss, in *The Alkaloids*, San Diego, CA, 1990, Vol. 37, p. 229.
2 H. L. Pearce, in *The Alkaloids*, San Diego, CA, 1990, Vol. 37, p. 145.
3 R. I. Owellen, C. A. Hartke, R. M. Dickerson and F. O. Haines, *Cancer Res.*, 1976, **36**, 1499.
4 L. Wilson, J. R. Bamburg, S. B. Mizel, L. M. Grisham and K. M. Creswell, *Fed. Proc.*, 1974, **33**, 158.
5 B. Botta, I. D'Acquarica, G. Delle Monache, D. Subissati, G. Uccello-Barretta, M. Mastrini, S. Nazzi and M. Speranza, *J. Org. Chem.*, 2007, **72**, 9283.
6 B. Botta, I. D'Acquarica, L. Nevola, F. Sacco, Z. Valbuena Lopez, G. Zappia, C. Fraschetti, M. Speranza, A. Tafi, F. Caporuscio, M. C. Letzel and J. Mattay, *Eur. J. Org. Chem.*, 2007, 5995.
7 B. Botta, M. Botta, A. Filippi, A. Tafi, G. Delle Monache and M. Speranza, *J. Am. Chem. Soc.*, 2002, **124**, 7658.
8 A. Tafi, B. Botta, M. Botta, G. Delle Monache, A. Filippi and M. Speranza, *Chem.–Eur. J.*, 2004, **10**, 4126.
9 B. Botta, D. Subissati, A. Tafi, G. Delle Monache, A. Filippi and M. Speranza, *Angew. Chem., Int. Ed.*, 2004, **43**, 4767.
10 B. Botta, F. Caporuscio, I. D'Acquarica, G. Delle Monache, D. Subissati, A. Tafi, M. Botta, A. Filippi and M. Speranza, *Chem.–Eur. J.*, 2006, **12**, 8096.
11 B. Botta, F. Caporuscio, D. Subissati, A. Tafi, M. Botta, A. Filippi and M. Speranza, *Angew. Chem., Int. Ed.*, 2006, **45**, 2717.
12 B. Botta, G. Delle Monache, C. Fraschetti, L. Nevola, D. Subissati and M. Speranza, *Int. J. Mass Spectrom.*, 2007, **267**, 24.
13 M. C. Letzel, C. Schäfer, F. R. Novara, M. Speranza, A. B. Rozhenko, W. W. Schoeller and J. Mattay, *J. Mass Spectrom.*, 2008, **43**, 1553.
14 (*a*) T. Su, *J. Phys. Chem.*, 1988, **88**(4102), 5355; (*b*) T. Su, *J. Phys. Chem.*, 1988, **89**, 5355.
15 J. F. Gal, M. Stone and C. B. Lebrilla, *Int. J. Mass Spectrom.*, 2003, **222**, 259.
16 C. B. Lebrilla, *Acc. Chem. Res.*, 2001, **34**, 653.
17 T. J. Wenzel, in *Discrimination of chiral compounds using NMR*, Wiley-Interscience, New York, NY, 2007, p. 278.
18 B. Botta, A. Tafi, F. Caporuscio, M. Botta, L. Nevola, I. D'Acquarica, C. Fraschetti and M. Speranza, *Chem.–Eur. J.*, 2008, **14**, 3585.
19 No significant B configuration effects have been observed in similar ligand displacements inside $\mathbf{4}_{R/S}$ hosts (see refs. 6,18).
20 V. Prakash and S. N. Timasheff, *Biochemistry*, 1991, **30**, 873.
21 S. Braun, H.-O. Kalinowski , S. Berger, *150 and More Basic NMR Experiments: A Practical Course*, 2nd expanded ed., Wiley-VCH, Weinheim, 1998, p. 205.
22 C. I. Bayly, P. Cieplak, W. D. Cornell and P. A. Kollman, *J. Phys. Chem.*, 1993, **97**, 10269.

